
*17th World Conference on Earthquake Engineering, 17WCEE*

*Sendai, Japan - September 13th to 18th 2020*

# INCORPORATING THE EFFECT OF DIRECTIVITY GROUND MOTIONS INTO HAZARD ASSESSMENT – A DIRECT AMPLITUDE-BASED APPROACH

KSK Karthik Reddy[1], Hing-Ho Tsang[2], Surendra Nadh Somala[3]

*(1) Ph.D. Scholar, Department of Civil Engineering, IIT Hyderabad & School of Engineering, Swinburne University of Technology, ce17resch01003@iith.ac.in*

*(2) Associate Professor, Swinburne University of Technology, Melbourne, Australia, htsang@swin.edu.au*

*(3) Assistant professor, Department of Civil Engineering, IIT Hyderabad, surendra@iith.ac.in*

## *Abstract*

The complex process of earthquake fault rupture leads to distinct characteristics of the ground motions due to different fault-styling and asperity positioning. One such peculiar feature is directivity. The phenomenon of directivity in earthquake rupture is represented in ground motions which are severe for stations along the propagation of rupture than stations in any other direction. This complex feature might break the circular symmetry, which alters the ground motion amplitudes from the typical pattern. Hence, ground motion directivity effects due to the kinematic characteristics of the fault need to be incorporated into seismic hazard assessment. This study aims to evaluate the effects of directivity on hazard assessment using the direct amplitude-based (DAB) approach. The DAB approach can incorporate the exact characteristics of directivity ground motions of each potential earthquake scenario. These directivity ground motions retain certain details of the fault configurations for each earthquake event. Such characteristics of ground motions are difficult to be incorporated through the conventional Cornell's approach of hazard assessment. The changes in the hazard curves with and without incorporating directivity ground motions are evaluated.

*Keywords: directivity; hazard curves; direct amplitude method.*



## 1. Introduction

The evidence of directivity ground motions was observed for 1994 Northridge, California, 1999 Chi-Chi, Taiwan, and 1999 Kocaeli and Duzce, Turkey, etc. The near field stations which are located in the direction of fault rupture and slip are classified as forward directivity stations [1]**.** The peculiar characteristics of these ground motions are identified by exploring the velocity-time histories which are associated with large amplitude and long period [2]. The velocity pulses resulting from rupture propagation superimpose and give rise to a single velocity pulse of high amplitude and natural period. The acceleration response spectra of such ground motions will show significant variation above natural periods of 0.6 sec [3]. This variation is not reflected in non-directivity ground motions where peaks in spectral content are sensed in lower natural periods. Such variation in response spectra is a threat to structures that tend to exhibit a higher natural period (i.e. bridges [4] and tall structures [5]). Hence these ground motions need to be treated with modification factors in advance before integrating into hazard assessment.

Deterministic seismic hazard analysis [6] and Probabilistic seismic hazard assessment [7] are ways of combating earthquakes by quantifying the rate of exceeding a certain ground motion at a site for all possible earthquake events. Such quantification of the return period of ground motions is a must while we consider designing critical structures (i.e. nuclear power plants [8], bridges [9])**.** While probabilistic seismic hazard analysis is an easy tool to evaluate the hazard, there are certain limitations as they do not consider the fault kinematics like the styling of the fault, positioning of nucleation asperity, etc. In the conventional PSHA, the ground motion intensity diminishes in a circular/elliptical pattern as we move away from the source, a result of which the ground motions at a particular site are either underestimated or overestimated. For instance, if a particular site is in front of the strike-slip fault and located towards the direction of rupture the ground motion is underestimated whereas it is overestimated in other directions. Limited studies accounted for the kinematics of the fault either at the level of performing the hazard assessment or at the level of ground motion equation.

Cornell's PSHA method [7 & 10] comprises of magnitude and distance integrals, and in order to account for the fault characteristics, additional integrals need to be included. Additional integrals though yield more accurate estimates of hazard, they add to the computational time effort as a result of an increase in complexity. The Direct Amplitude Based (DAB) introduced by Tsang, H. H [15] doesn't require additional integrals as the spectral amplitudes are treated with modification factors and a recurrence relationship among the amplitudes is established to carry out hazard assessment. Spagnuolo [11] shaped an additional 3 variables, one to account for angles describing the focal mechanism, a second parameter associated with the rupture velocity and a final parameter to represent the position of hypocentre location. For faults with uncertainty concerning this parameter information, a uniform distribution is assumed. A comparison of Cornell PSHA analysis, with and without these additional variables, for strike-slip fault propagating unilaterally, exhibited an increment of 100% for certain sites. For the case where the ground motion equation needs to be shaped to contain these parameters biased ground motion equations for near field accounting for the forward directivity effects are employed[12]. The contours [12] clearly portray significantly higher ground motion intensities for stations tapered at the end of fault than any other orientation around the fault.

## 2. Generation of the Earthquake Catalogue

In order to facilitate the earthquake catalogue, an area of 1000 $km^2$ is selected (Fig. 1). The earthquake events follow a Gutenberg-Richter relationship of the order 0.71 depicting the seismic activity in central Himalayas [13]. The annual recurrence of 4 magnitude earthquake events is 4.227 and for 5 magnitude events is 0.815. Subsequently, earthquake events of 6 magnitudes are 0.157 and the events of 7 and 8 are 0.03 and 0.006 respectively. The events of magnitude 6 and above are distributed in the domain following a normal distribution with the center of the domain as mean. A standard deviation is applied in such a way that the events fall inside the square domain and do not surpass the area boundaries. Events of magnitude 7 and 8 are considered along the Himalayan belt with a strike angle orientation of 15º. The faults of these events are placed closer to the station to create the maximum directivity effect. The generated earthquakes also imitate the



 

distribution of events in the Nepal region. Nepal region is susceptible to high seismicity hence the existing hazard curves[19] can be used as a check to the reported uniform hazard spectrum in this study.

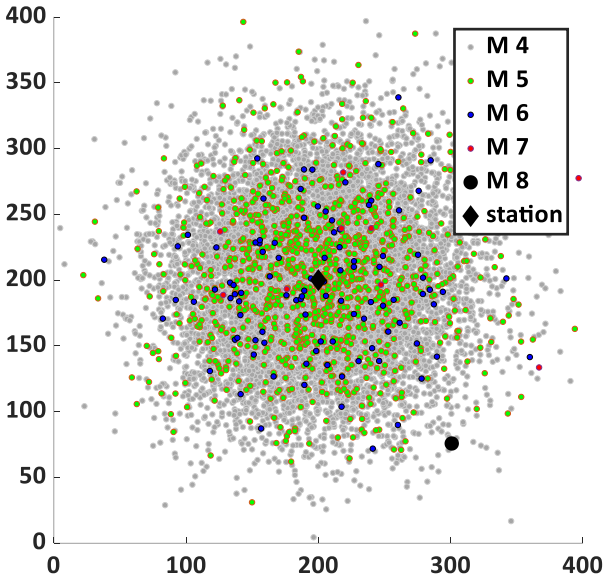


Fig. 1 – Earthquake catalogue containing magnitude from 5 to 8 normally distributed in the domain

## 2.1 Proportionating finite fault dimensions from point source events

Ground motion prediction equations (GMPE's) are employed to obtain the response spectra at a station due to a particular event. The obtained response spectra need to be altered by the application of a post-factor to contain the directivity effect. In order to apply the post-factor correction, each point source needs to be treated as a finite-fault according to scaling relations (Magnitude-Length) proposed by Wells & Coppersmith [14]. Eq. (1) gives the relationship between the magnitude and length of the fault, from which the surface length of the faults can be back-calculated as in Eq. (2). The subsequent step followed is the application of the post-factor based on fault dimensions and site location relative to the fault and hypocenter.

$$M = 5.16+1.12 \times \log(L) \quad \text{(strike-slip rupture)} \quad (1)$$

$$L = 10^{(-3.55+0.74 \times M)} \quad \text{(strike-slip rupture)} \quad (2)$$

## 2.2 Generation of directivity and non-directivity response spectra

Application of the Direct amplitude method (DAB) to compute the hazard curve needs an acceleration response spectra database at the station of interest for all the events. Two ground motion prediction equations were used to generate the non-directivity response spectra database. Boore Atkinson attenuation relation [18] is used to compute the average horizontal spectrum from periods 0.01s to 10s. This GMPE is used abundantly around the world for the active seismic region as it also accounts for the styling of the fault, as well as shear wave velocity (Vs30) and the minimum distance of the fault source to the station of interest. Iyengar and Raghukanth [17] GMPE is used to obtain ground motions for stable regions, owing to its applicability to ground motion intensities for peninsular India. The weighted average of these equations was considered to obtain the non-directivity motion database.

### 2.2.1 Application of Post-Factor Based on Somerville (2013)

Directivity post factors were initially prescribed by Somerville [18] wherein correction factors were applied based on station orientation with respect to the fault, the details of which are described in next-generation attenuation (NGA-2) report. According to Somerville [18], the spectral content of any event can be converted to directivity ground motion by adding this factor to the logarithm of spectral acceleration. The factor is given



 

in Eq. (3) depends on input parameters like fault geometry, the proportion of rupture length between the hypocentre and the fault. Tapering coefficients for magnitude, distance and azimuth are additionally applied to account for the orientation of the station with respect to the fault. Post-factors were suggested for the strike and dip-slip fault, wherein faults with rake angle between 0 to $30^0$ are classified as strike-slip faults. Fig. 2 describes the geometric assumptions used to evaluate this factor.

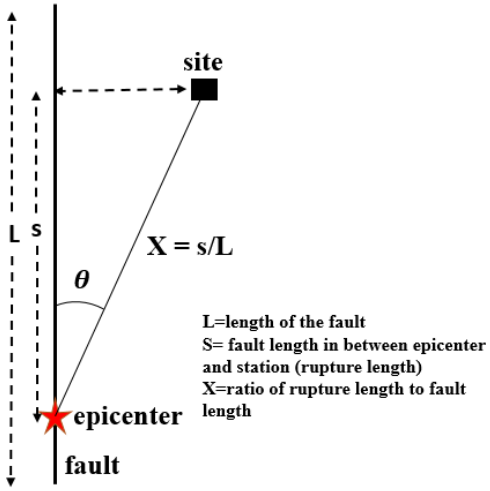


Fig. 2 – Geometric assumptions to account for source rupture directivity (after Somerville et al., 1997).

$$f_d = (C_0 + C_1 \times f_{geom}) \times T_{cd} \times T_{Mw} \times T_{az} \quad (3)$$

$$f_{geom(s,\theta)} = \log(s) \times (0.5\cos(2\theta) + 0.5) \quad (4)$$

$f_{geom}$ takes the azimuth of the station with respect to the fault into consideration, in case the station lies in the line of the fault the $f_{geom}$ attains the maximum value. The term also contains a logarithm of $s$ value which depends on the length of the fault surface between the station of interest and epicenter. The impact of these factors can be studied by considering a hypothetical case of a fault generating 8 magnitude earthquake with epicenter at the extreme end of the fault. Such a fault can produce a maximum directivity amplification factor as high as 4. In such cases, a kink can be observed in response spectra as a result of adding directivity factor to non-directivity spectral amplitudes.

The coefficients recommended by Somerville [18] also account for non-directivity stations where there is a decrease in spectral amplitudes on the application of these factors. Such a trend can be observed for the station which lies away from the fault with an azimuth higher than 45 degrees. Further, the post-factor is treated with magnitude taper, such that earthquakes of higher magnitude produce a higher magnitude taper when compared with earthquakes of low magnitudes. Hence, earthquakes with magnitudes less than 5 can be discarded, and earthquakes of magnitudes 6.5 and above do not alter the magnitude taper factor [18]. Magnitudes in between 6.5 and 5 linearly decrease from 1 to 0. Similar treatment is done for distance and azimuth taper as well [18].

Fig. 3(a) shows the variation in spectral content with the application of post-factor for a 7 magnitude earthquake. Similar factors were applied for an 8 magnitude earthquake and presented in Fig. 3(b). It can be observed that station oriented along strike (also referred to here as 0-degree site angle) produces higher spectral acceleration compared to generic Boore-Atkinson attenuation relationship. Although the 45-degree azimuth shows lower spectral acceleration for Mw7, there isn't a significant difference from the Magnitude 8 earthquake (Fig. 3).



 

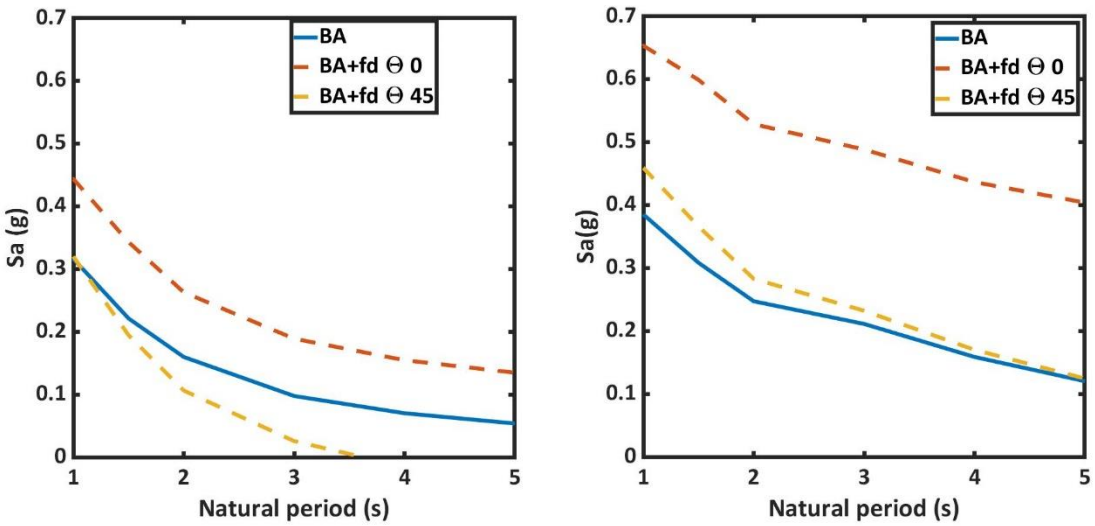


Fig. 3 –Variation in spectral acceleration for (a) 7 magnitude and (b) 8 magnitude earthquakes with corresponding modification factors. Blue legend represents the response spectra generated using BA (2008) ground motion prediction equation. Red legend shows the increase in spectral amplitudes for a station lying at a distance of 10km from the fault with a 0° site angle (along-strike). Yellow indications that spectral amplitudes decrease for the same station when oriented at a 45° site angle.

## 3. Direct Amplitude-Based (DAB) Approach

The direct amplitude-based approach is derived analytically from Cornell's source-based approach, where probability distribution functions (PDF) are defined for magnitude and distance to the corresponding station for an earthquake event (i). The PDF is derived from cumulative distribution functions (CDF). The obtained PDF is integrated for a range of magnitudes and distances as shown in Eq (5) and the corresponding ground motion intensity is obtained. The ground motion is multiplied with a rate of occurrence $\vartheta_i$ depending on the earthquake source. The probability of the obtained ground motion exceeding a particular value is evaluated at various natural periods (T) and hazard curves are plotted for various return periods.

$$\mathrm{V[z]} = \sum_{i=1}^{N_s} \vartheta_i \int_{m=m_0}^{m=m_u} \int_{r=0}^{r=\infty} P[Z > z|m,r] f_i(m) f_i(r) dr dm. \quad (5)$$

$$P[Z > z] = 1 - e^{-v(z)T} \leq \mathrm{v(z)T} \quad (6)$$

The direct amplitude-based approach considers all the events as individual sources $N_s$, the spectral response amplitudes (Δ) for all the events are treated with modification factors (either source or site ). A CDF is defined to account for amplitude recurrence relation from which a PDF is established for the mean amplitude and integrated between maximum $\Delta_{max}$ and minimum amplitudes $\Delta_{min}$. The probability of obtained amplitude exceeding is calculated in a similar cornel PSHA manner which is then multiplied with N(Δmin) the mean annual rate of the median amplitude (Δ) exceeding the minimum value (Δmin). The description in the equation form is as follows. The steps followed in the DAB method are illustrated in Fig. 4.

$$\mathrm{V[z]} = N(\Delta_{min}) \int_{\Delta=\Delta_{min}}^{\Delta=\Delta_{max}} P[Z > z|\Delta] f(\Delta) d(\Delta) \quad (7)$$



 

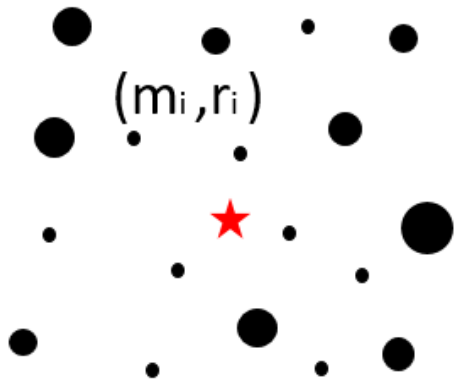


Step 1: Earthquake Catalog

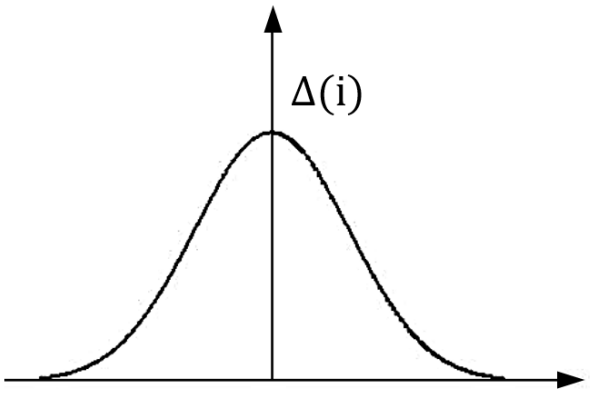


Step 2: Ground Motion Attenuation Modeling for Each Event

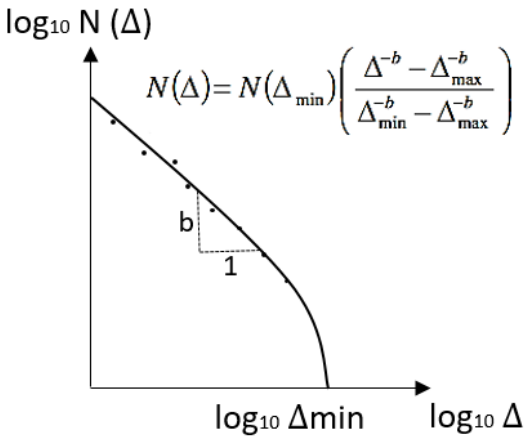


Step 3: Amplitude Recurrence Relationship

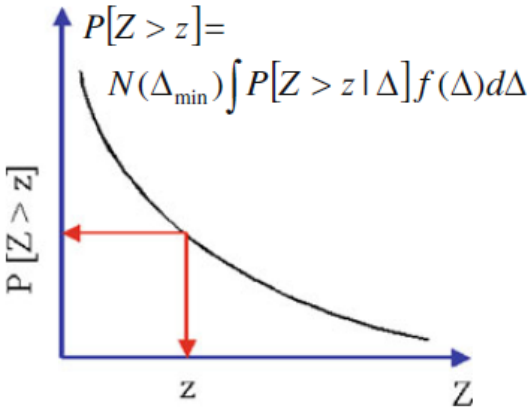


Step 4: Seismic Hazard Curve

Fig. 4 - Steps involved in the direct amplitude-based (DAB) approach of PSHA (Tsang and Chandler [16])

## 4. Discussions

The plot in Fig. 5 shows the hazard curves obtained for non-directivity (ND) and directivity (D) ground motions after the application of the post-factor. Since the directivity factor alters the spectral amplitudes above 0.5 secs return periods of spectral accelerations are plotted for two natural periods (1.5 sec and 5 secs). The trend followed by the directivity hazard curve is in line with the non-directivity hazard curve for lower periods but delineation is observed from natural periods above 1 sec.

The reduction in the return period for directivity hazard curve can be vividly observed for both the selected natural periods. The dominance of the directivity factor in the hazard curve is quite significant. The significance intensifies with an increase in the natural period. The continuous line in Fig. 5 is a non-directivity hazard curve, while the dotted line is for directivity. The difference in directivity and non-directivity hazard curves though substantial for a natural period of 1.5 sec, is much higher for a 5 sec natural period.

The reported spectral amplitude at the natural period of 1.5 sec is 0.6g in a non-directivity scenario, it shifts to 0.74g in directivity scenario for a return period of 475 years. An increment from 0.09g to 0.2g is observed at 5 secs for the same return period. A 100% percentage increment is observed at 5 sec, similar values have been reported by [11] for the station in front of the fault.



 

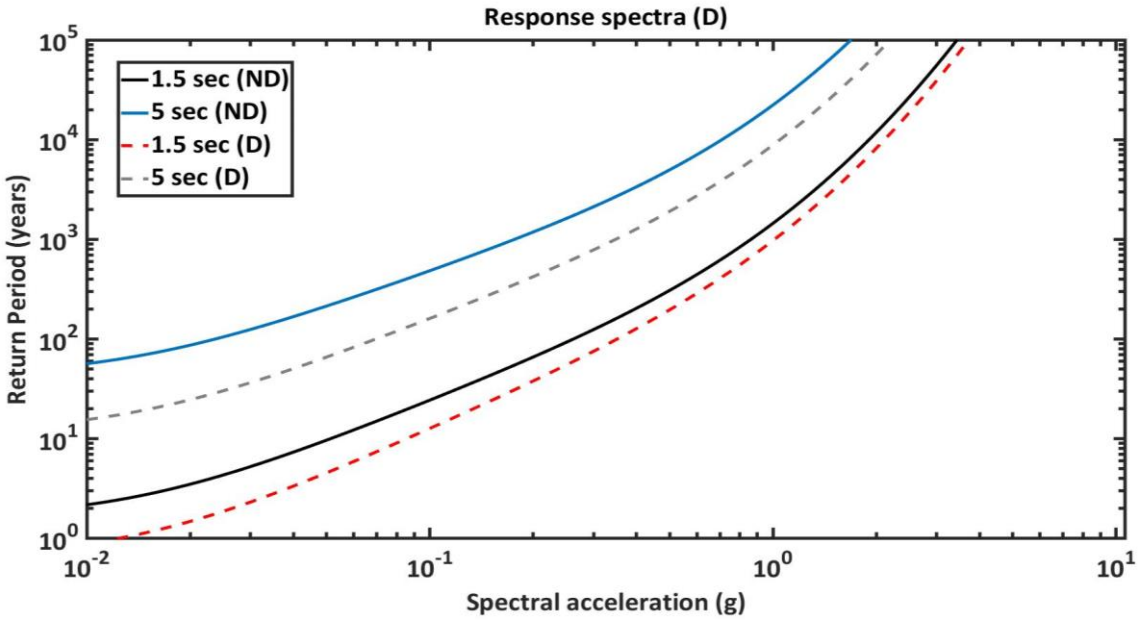


Fig. 5 - Hazard curves for the selected natural periods using DAB approach for directivity and non-directivity spectral amplitudes.

In order to explore this peculiar behaviour of directivity in the hazard curve, the response spectra from the hazard curve are plotted from natural periods of 0.1 sec to 10 secs in Fig. 6.

In Fig. 6 (a) the uniform hazard curve is plotted for a return period of 72 years. The peak spectral amplitude was observed at 0.3 sec reportedly 0.5g. The deviation in the hazard curves is visible from 0.5 sec until which both the curves follow similar trends, beyond that at 1.5 sec the reported spectral amplitude is 0.2g while it nears to 0.3g upon application of the post-factor, an increment of 50% is observed. While an increment of 42% percentage is observed at 2 sec. A 100% percentage of increase can be sensed at natural periods beyond 3 sec, as a rough estimate, a modification factor of 1.5 can positively be applied for spectral amplitudes between 0.5 and 2, while a factor of 2 can serve the need of converting the non-directivity hazard spectra to directivity hazard spectra for a return period of 72 years.

Fig. 6 (b) is a comparison of hazard spectra between directivity and non-directivity case for a return period of 475 years, an increment of 12% and 25% is observed at 1 sec and 1.5 sec respectively. The reported spectral amplitude shifted from 0.6g to 0.74g for 1.5 sec natural period. At 2 sec there is an increment of 50%, beyond which there is a progressive increment varying from 50% to 100% until 5 sec. A logarithmic increment is recommended while applying modification factors to convert non-directivity hazard curves to directivity hazard curves for a return period of 475 years. The factor begins with 1.15 at 1 sec natural period, followed by 1.25 at 1.5 sec and 1.5 at 2 sec. A constant factor of 2 is applied beyond 2 sec for the rest of the natural periods.

Fig. 6(c) hazard curve is plotted for a return period of 2475 years, the reported peak spectral amplitude is 2.04g. An increment of 15% and 18% is observed in spectral amplitudes at 1 sec and 2 sec respectively. While an increment of 30% was observed at 3 sec, it slowly ascends to 40% for 4 sec beyond which 72% increment was observed at 5 sec. As the return period increases the increment to convert non-directivity to directivity ground motion lessens.

The hazard curves of directivity and non-directivity tend to converge at higher return periods beyond $10^5$ years as shown in Fig. 5. hence there is a reduction in percentage increment with an increase in the return period. However, a substantial amplification is evidently observed for higher return periods. A low value of shear wave velocity ($V_{S30}$=200 km/s$^2$) was considered in generating the spectral amplitudes database, hence resulted in overestimating the hazard spectra.



 

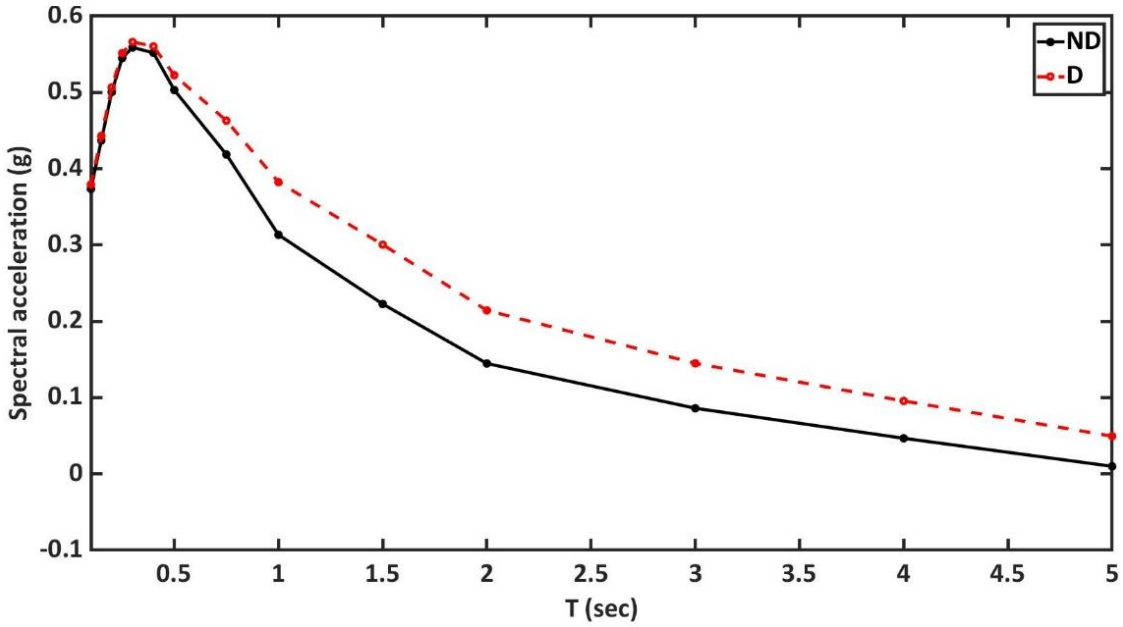


Fig. 6(a) – Hazard curve for a return period of 72 years using the DAB approach for directivity and non-directivity spectral amplitudes.

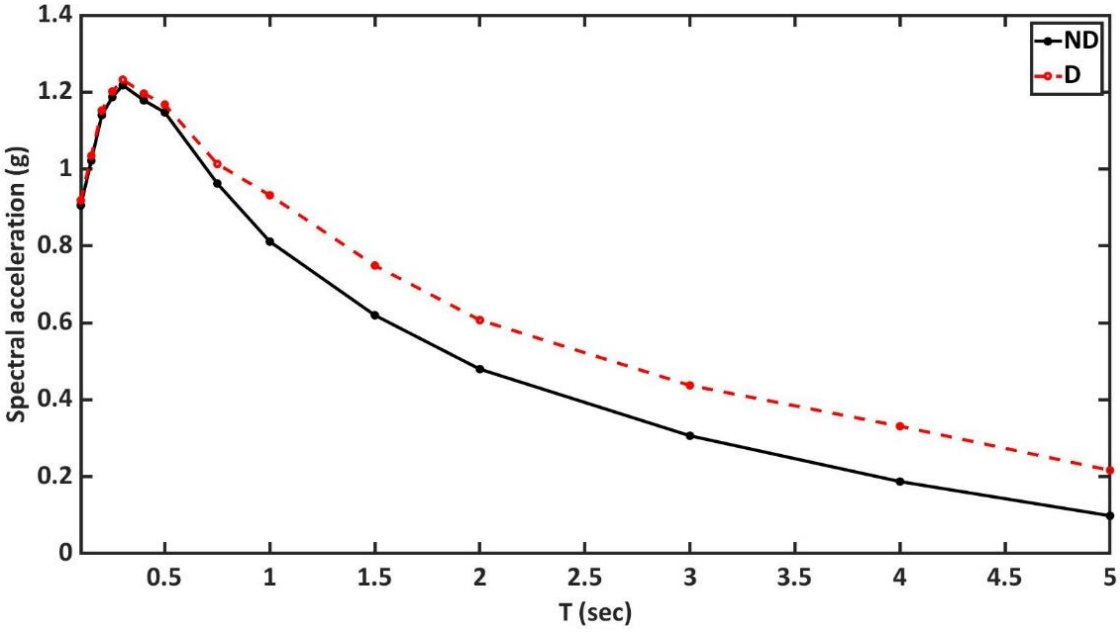


Fig. 6(b) – Hazard curve for a return period of 475 years using the DAB approach for directivity and non-directivity spectral amplitudes.



 

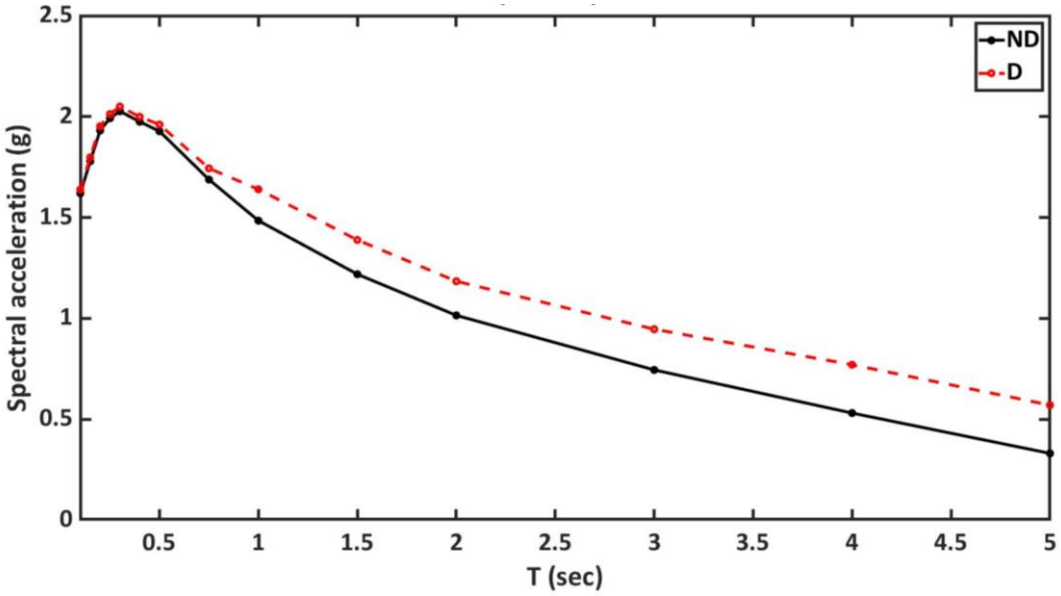


Fig. 6(c) - Hazard curve for a return period of 2475 years using the DAB approach for directivity and non-directivity spectral amplitudes.

## 5. Conclusions

- Somerville directivity post factors used to treat non-directivity ground motions tend to increase the spectral amplitudes at higher natural periods.
- The shift of amplitude at higher natural periods is clearly reflected in the hazard response spectra. A direct amplitude-based approach seemingly is an essential and simple tool that can be used to carry out a hazard assessment to account for directivity effects.
- An increment in spectral amplitudes is higher for lower return periods. The incremental factor in spectral amplitudes for a return period of 72 years is in the order of 1.5 for natural periods less than and equal to 2 sec, beyond which it is 2.
- The incremental factor in spectral amplitudes for a return period follows a logarithmic increment that begins with 1.12 at the natural period of 1 sec, followed by 1.25, 1.5 and 2 for subsequent natural periods of 1.5, 2 and beyond 2 respectively.
- A linear increment beginning from 15 % to 40% is observed for natural periods until 4 sec while a sudden increment of 70% is observed at 5 sec natural period for a return period of 2475 years.
- A low value of shear wave velocity at the GMPE's level has resulted in overestimated values of hazard spectra but the ratio between the three return periods is around 1.8-2.2, which is typical for a high seismic region.
- Irrespective of the reported peak spectral amplitudes, the incremental factors suggested can be considered as a benchmark to gauge the hazard due to directivity as the hazard curves are obtained for a complete earthquake catalogue.

## 6. Acknowledgments

This study is funded by the Ministry of Earth Sciences (MoES), India under grant number MoES/P.O.(Seismo)/I(304)/2016.

## 7. Copyrights

## 8. References

[1] Somerville, P. G., Smith, N. F., Graves, R. W., & Abrahamson, N. A. (1997). Modification of empirical strong ground motion attenuation relations to include the amplitude and duration effects of rupture directivity. Seismological Research Letters, 68(1), 199-222.

[2] Somerville, P. G. (2003). Magnitude scaling of the near-fault rupture directivity pulse. Physics of the earth and planetary interiors, 137(1-4), 201-212.

[3] Bray, J. D., & Rodriguez-Marek, A. (2004). Characterization of forward-directivity ground motions in the near-fault region. Soil dynamics and earthquake engineering, 24(11), 815-828.

[4] Li, S., Zhang, F., Wang, J. Q., Alam, M. S., & Zhang, J. (2017). Effects of near-fault motions and artificial pulse-type ground motions on super-span cable-stayed bridge systems. Journal of Bridge Engineering, 22(3), 04016128.

[5] Zhang, Y., & Iwan, W. D. (2002). Active interaction control of tall buildings subjected to near-field ground motions. Journal of Structural Engineering, 128(1), 69-79.

[6] Kolathayar, S., Sitharam, T. G., & Vipin, K. S. (2012). Deterministic seismic hazard macrozonation of India. Journal of earth system science, 121(5), 1351-1364.

[7] Cornell, C. A. (1968). Engineering seismic risk analysis. Bulletin of the seismological society of America, 58(5), 1583-1606.

[8] Klügel, J. U. (2005). Problems in the application of the SSHAC probability method for assessing earthquake hazards at Swiss nuclear power plants. Engineering Geology, 78(3-4), 285-307.

[9] Alameddine, F., & Yashinsky, M. (2006). Seismic Hazard for California Bridges Using Deterministic and Probabilistic Methods. In Fifth National Seismic Conference on Bridges & Highways Multidisciplinary Center for Earthquake Engineering Research California Department of Transportation Federal Highway Administration Transportation Research Board (No. B10).

[10] Baker, J. W. (2008). An introduction to probabilistic seismic hazard analysis (PSHA). White paper, version, 1, 72.

[11] Spagnuolo, E., Herrero, A., & Cultrera, G. (2012). The effect of directivity in a PSHA framework. Geophysical Journal International, 191(2), 616-626.

[12] Akkar, S., Moghimi, S., & Arıcı, Y. (2018). A study on major seismological and fault-site parameters affecting near-fault directivity ground-motion demands for strike-slip faulting for their possible inclusion in seismic design codes. Soil Dynamics and Earthquake Engineering, 104, 88-105.

[13] Shubham, D. S. (2018). Earthquake Hazard Update in Central Himalaya. Geosciences, 8(1), 1-6.

[14] Wells, D. L., & Coppersmith, K. J. (1994). New empirical relationships among magnitude, rupture length, rupture width, rupture area, and surface displacement. Bulletin of the seismological Society of America, 84(4), 974-1002.

[15] Tsang, H. H., & Chandler, A. M. (2006). Site-specific probabilistic seismic-hazard assessment: direct amplitude-based approach. Bulletin of the Seismological Society of America, 96(2), 392-403.

[16] Boore, D. M., & Atkinson, G. M. (2008). Ground-motion prediction equations for the average horizontal component of PGA, PGV, and 5%-damped PSA at spectral periods between 0.01 s and 10.0 s. Earthquake Spectra, 24(1), 99-138.

[17] Iyengar, R. N., & Kanth, S. R. (2004). Attenuation of strong ground motion in peninsular India. Seismological Research Letters, 75(4), 530-540.

[18] Spudich, P., Bayless, J. R., Baker, J. W., Chiou, B. S., Rowshandel, B., Shahi, S. K., & Somerville, P. (2013). Final report of the NGA-West2 directivity working group.

[19] Chaulagain, H., Rodrigues, H., Silva, V., Spacone, E., & Varum, H. (2015). Seismic risk assessment and hazard mapping in Nepal. Natural Hazards, 78(1), 583-602.



 